Radiation Protection Dosimetry (2011), Vol. 146, No. 4, pp. 383–394
Advance Access publication 8 June 2011
doi:10.1093/rpd/ncr238

NEUTRON SPECTROMETRY WITH BONNER SPHERES FOR AREA MONITORING IN PARTICLE ACCELERATORS

Roberto Bedogni*
INFN-LNF Frascati National Laboratories, Via E. Fermi n. 40-00044, Frascati (RM), Italy

*Corresponding author: roberto.bedogni@lnf.infn.it

Selecting the instruments to determine the operational quantities in the neutron fields produced by particle accelerators involves a combination of aspects, which is peculiar to these environments: the energy distribution of the neutron field, the continuous or pulsed time structure of the beam, the presence of other radiations to which the neutron instruments could have significant response and the large variability in the dose rate, which can be observed when moving from areas near the beam line to free-access areas. The use of spectrometric techniques in support of traditional instruments is highly recommended to improve the accuracy of dosimetric evaluations. The multi-sphere or Bonner Sphere Spectrometer (BSS) is certainly the most used device, due to characteristics such as the wide energy range, large variety of active and passive detectors suited for different workplaces, good photon discrimination and the simple signal management. Disadvantages are the poor energy resolution, weight and need to sequentially irradiate the spheres, leading to usually long measurement sessions. Moreover, complex unfolding analyses are needed to obtain the neutron spectra. This work is an overview of the BSS for area monitoring in particle accelerators.

INTRODUCTION

Particle accelerators represent a very important environment for the development of the radiation protection field. It is at accelerators 'that the science and technology of radiation dosimetry are at their most sophisticated'[1] and neutron dosimetry is certainly behind much of this complexity[2]. While the dosimetry of photons is simplified by the convention that the quality factor is 1 for all energies[3], the determination of the operational quantities for neutrons is more complex, because the spectrum of neutron-induced secondary particles in tissue is complex and difficult to mimic with instruments, relying on nuclear reactions generally different from those occurring in tissue. The degree of complexity is increased by the large variability of neutron energies in particle accelerator workplaces, spanning from thermal neutrons (10^{-8} MeV) to hundreds or thousands of MeV.

At electron accelerators, the photoneutrons ($\sim$ MeV), produced by the giant dipole resonance (GDR) interaction, is the dominating component[4]. Nevertheless, if the energy of the primary particle exceeds the thresholds for the quasi-deuteron ($\sim$25 MeV) or photo-pion (200 MeV) effects, higher energy neutron components are produced in the intervals between 10 and 100 MeV (pseudo-deuteron effect) or $E >$100 MeV (photo-pion effect). Owing to its penetration capability, the latter component and its secondary field of lower energy neutrons and photons dominate the radiation environment behind thick concrete shields. As shown in Figure 1, the near-target field is dominated by GDR neutrons, while the spectrum behind thick concrete shield presents an important high-energy component that tends to accumulate in the 10^2 MeV region, corresponding to the minimum cross section for most materials.

For proton facilities with energy above $\sim$10 MeV, neutrons usually constitute the main hazard in areas accessible to workers. The neutron-producing mechanisms are diverse: (p,n) reactions dominate the low-energy range ($E_p < 200$ MeV), whereas a number of neutron-producing reactions become possible in the intermediate energy region (200 MeV $< E_p <$ 1 GeV). Here the neutron production occurs via evaporation ($1 < E_n < 10$ MeV) or hadronic cascade ($E_n > 10$ MeV). An increased number of reactions produces high-energy neutrons when $E_p > 1$ GeV. A more detailed characterisation of workplace spectra at proton accelerators is given in ref. (5).

A common point to high-energy electron or hadron facilities is that if primary particles have enough energy to trigger the nuclear cascade, the neutron spectra produced in shielded areas are very similar. This is shown in Figure 2, where the neutron spectra produced behind the lateral shield of an electron facility and a hadron facility are compared. In the electron case, the 3-GeV beam hits a Cu target and the lateral concrete shield is 50 cm thick. The hadron case is the CERF[6] (CERN-EU high-energy reference field facility), where a 120-GeV proton beam impinges on a thick copper target and the concrete shield is 80 cm thick.

Ideally, the fluence response of an instrument (reading per unit incident fluence) as a function of

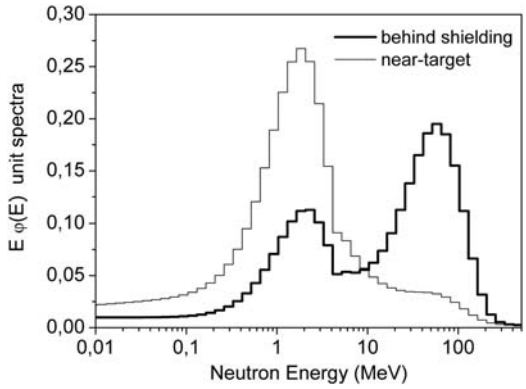

Figure 1. Neutron spectra normalizsed to the unit fluence (unit spectra) at 90° from a copper target irradiated with 3 -GeV electrons, in the target area and behind a 50-cm thick concrete shielding (data simulated with FLUKA and interpolated with continuous functions).

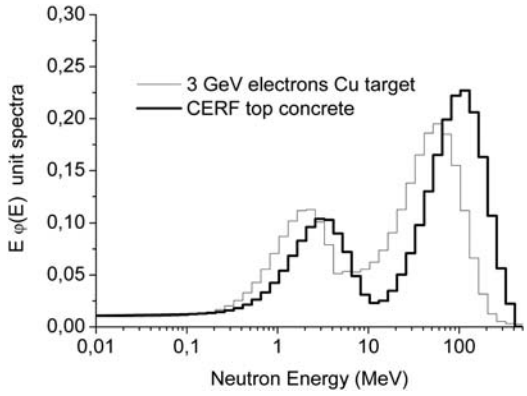

Figure 2. Unit neutron spectra behind lateral concrete shields for different facilities: a 3-GeV electron beam on a copper target (courtesy M. Pelliccioni) and the CERF (120 120-GeV protons on copper target)—concrete top.

the neutron energy should be proportional to the fluence-to-ambient dose equivalent conversion coefficients established by ICRP and ICRU[7, 8], but the variation of these coefficients with neutron energy is as large as a factor of 40 from 1 keV to 1 MeV. A consequence is that the performance of neutron-measuring instruments as a function of the energy is usually poor, leading to over- or under-estimations if the instrument is used in a field having an energy distribution different from that of the calibration field.

As far as the area monitoring is concerned, instruments with reasonably flat dose equivalent response have been developed[9], but only within a restricted energy sub-interval. Commonly employed rem-

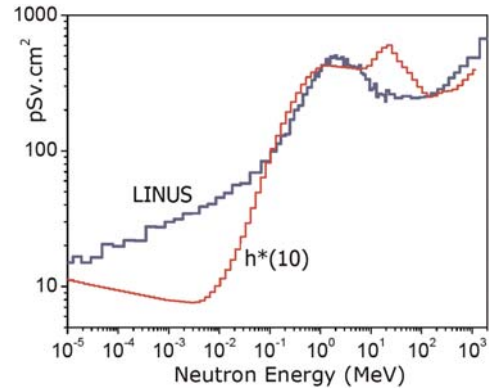

Figure 3. Energy dependence of the fluence response of the LINUS spherical counter (courtesy M. Silari) compared with the fluence-to-ambient dose equivalent conversion coefficient.

counters, based on a thermal detector in the centre of a moderating sphere, usually show satisfactory energy response in the mega-electronvolt region (corresponding to the energy of the calibration sources), but their performance at intermediate energies and >20 MeV is poor. To enhance their high-energy response, heavy metal layers have been included in the moderator[10–12] (extended range rem-counter), but even this modification does not guarantee that the fluence response is fully proportional to the relevant conversion coefficient (see Figure 3). Once again, the application of workplace-specific correction factors is required if the workplace spectrum differs significantly from the calibration spectrum. TEPC-based instruments, which infer the total $H^*(10)$ on the basis of measured microdosimetric spectra, have been also used in high-energy neutron fields with satisfactory results[13]. A recent intercomparison of survey instruments was organised at the GSI in the framework of the CONRAD project (COordinated Network for RAdiation Dosimetry, funded by the European Commission within its 6th Framework Programme). Here, extended range rem-counters and TEPC instruments were exposed in the field produced behind a thick concrete shield by a 400-MeV/nucleon carbon beam hitting a graphite target. Both types of instruments were able to determine the neutron component of $H^*(10)$ with an accuracy in the order of 10 % or better[14].

A variety of passive detection techniques, widely used in personal dosimetry[15, 16], have also been employed in survey instruments. For the high-energy neutron fields encountered at particle accelerators, thermoluminescence dosimeter (TLD) pairs or nuclear track detectors have been used in the centre of an extended range sphere (passive LINUS). Recently, single moderator multidetector passive

instruments with spectrometric capabilities from thermal to 20 MeV have been developed[17, 18]. They are promising for radiation monitoring purposes, but further studies are needed to extend the response to higher energy and to provide real-time readings.

There are exhaustive reviews of neutron dosimetry techniques[16] and their application in accelerator-based workplaces[4], and all of them recommend the use of spectrometry techniques[19] to support workplace neutron dosimetry for the following reasons:

(1) For evaluating the suitability of a given instrument, or its response as a function of the energy, for a specific workplace and to determine workplace-specific correction factors[20].
(2) For identifying relevant points of the installation where the neutron field can be fully characterised through spectrometry and/or calculation, and that can be employed as simulated workplace neutron fields[21, 22] for the calibration of survey instruments and dosemeters to be used in the installation.
(3) Although the operational quantities were designed to provide a conservative estimation of the effective dose, there are neutron energies and irradiation geometries where the differences are significant, leading to relevant over- or under-estimation of the effective dose[23]. Consequently, even if the operational quantities are correctly estimated, spectrometric information may be needed in some circumstances, e.g. when exposures approach the limits.

If the neutron spectrum is known, $H^*(10)$ in workplaces may be derived by the following calculation:

$$H^*(10) = \int_{E_{\min}}^{E_{\max}} \mathrm{d}E \cdot \Phi(E) \cdot h^*_{\varphi}(E) \qquad (1)$$

where $\Phi(E)$ is the energy distribution of the neutron fluence and $h^*_{\phi}(E)$ is the fluence-to-ambient dose equivalent conversion coefficient.

The Bonner sphere spectrometer (BSS) is certainly the most used spectrometer for radiation protection applications due to a number of advantages:

– The wide energy range: to date, the BSS is the only system that is able to cover the whole range of energies encountered in particle accelerators[24]. A set of five to six well-chosen polyethylene spheres with diameter ranging from 2 in. to 12 in. is adequate for neutron energies up to 20 MeV[25]. If higher energy components have to be measured, extended range spheres are added[26, 27].
– Different types of thermal neutron detectors can be used as the central sensor of the BSS. At INFN-LNF the same set of spheres, including three extended range spheres, has been used with a ^{6}LiI(Eu) scintillator[28, 29], TLD pairs[30, 31] and gold[30, 32] or dysprosium activation foils[33, 34] for measurements in particle accelerators under different conditions of intensity, time structure and intensity of the photon fields. An appropriate choice of the thermal detector may allow the BSS to work correctly even in the presence of very intense photon fields as in electron accelerators.
– The acquisition system is usually simple and is based on a spectrometric or counting chain for active counters. For passive detectors, like activation foils, TLD pairs or nuclear track detectors, the detector has to be removed from the sphere after the irradiation, and then analysed. The analysis may take place '*in situ*' for activation foils, if portable counting systems (NaI(Tl) or beta counters) are available.
– The isotropy of the response, helping in the determination of the fluence and of $H^*(10)$.
– Accuracy: in the above-mentioned CONRAD inter-comparison[35], where >40 % of the neutron component of $H^*(10)$ was due to neutrons >20 MeV, three different BSSs with extended range (ERBSS) having different thermal neutron detector, response matrix, calibration and unfolding codes provided very consistent results in terms of fluence and ambient dose equivalent.

A limitation is the poor energy resolution due to the shape of the response functions that are characterised by similarities and overlapping. Particularly, the best energy resolution is in the interval between 0.1 and 20 MeV, corresponding to the maximum degree of differentiation of the response functions, whereas poor resolution is found in the intermediate energy region and >20 MeV[36], where all response functions tend to have similar slopes. As a general rule, neutron spectra having a smooth and continuous shape can be well described by a BSS, while the fluence associated with narrow peaks or fine structures will be spread over a larger energy interval.

The weight and the large volume entailed by a set of spheres are further limitations. In addition, the spheres need to be sequentially irradiated, usually leading to long measurement sessions. Furthermore, monitoring instruments working in parallel with the BSS are needed when the field varies over time.

Provided that a well-established and validated response matrix is available, usually derived from Monte Carlo simulations, the most complex aspect of the spectrometry task is the unfolding process, due to the non-uniqueness of the mathematical solution. This requires the introduction of a certain amount of '*a priori*' information, which has to be taken into account in the unfolding process.

An experimental difficulty, especially for large spheres, is the need to irradiate the spectrometer uniformly, which is the condition under which the response functions are calculated. This condition is fulfilled with point sources at large distances. In collimated fields, beam-scanning techniques have to be implemented, or a response matrix specially calculated for a partial irradiation condition has to be used[34]. It should be noted that the 'uniform irradiation condition' does not necessarily imply an aligned expanded field: any angular distribution is allowed, since the sphere response is isotropic.

Besides the measurement problems due to the variability of the neutron energy in workplaces, relevant aspects of accelerator-based workplaces are the time structure, which is frequently sharply pulsed, the large variability in the dose rate, which can be observed when moving from areas near the beam line to free access areas and the presence of other radiations to which the neutron instruments could have significant response. All these aspects may have an impact on the response of survey instruments and of the BSS.

Because exhaustive literature on the BSS and its use in radiation protection is available[24, 25, 37], this work will treat only a limited number of aspects that are of particular interest in particle accelerator monitoring, particularly, the choice of the thermal neutron detector in relation to the field intensity and the time structure, the response matrix, the choice of the moderating spheres, the uncertainties and the unfolding procedures.

THE RESPONSE OF THE BSS

The response function of a sphere, defined as the reading per unit fluence as a function of the monoenergetic neutron energy, under uniform irradiation condition, is usually derived by Monte Carlo simulations. The simulation is frequently done with a parallel field having the same diameter as the sphere. The calculated response will be adequate for measurements in fields with any directional distribution, provided that the irradiation of the sphere is uniform. Various transport codes are suited to calculate the response matrix of a BSS. A recent computational exercise[38] organised in the framework of the CONRAD project demonstrated that the MCNP family is used in the majority of the cases. FLUKA[39, 40] and GEANT 4[41] have also been used, obtaining comparable results. Accurate (within few per cent) response function calculations can be done from thermal to 20-MeV neutrons, because the cross-sectional libraries are well established in this energy range. Above 150 MeV the simulation codes employ models, due to the limited amount of measured data available. However, experiments with spallation targets[42], the recent CONRAD comparison[43] and BSS validation experiments performed at the CERF facility[44], suggest that such models may be regarded as accurate enough for these purposes.

The number of monoenergetic energies needed to accurately simulate a sphere must be consistent with the complexity of the response function. Fine structures such as narrow resonances should be resolved by reducing the width of the energy intervals: this is the case with designs including cadmium layers. In the absence of such structures, the response of a sphere can be accurately simulated using a 50–100 bin energy structure. Dimensions and densities of the materials constituting the BSS should be accurately measured and implemented in the simulation model. The importance of an accurate knowledge of the polyethylene density is shown in ref. (37), where the relative change in the sphere response due to changes in the polyethylene density, $(dR/R)/(d\rho/\rho)$, is calculated as a function of the neutron energy and the sphere diameter. This quotient can be as high as 6 and increases in energy regions where the sphere response is poor.

The accuracy of the response matrix can be evaluated through irradiations in monoenergetic or broad-spectrum reference fields (<20 MeV) as those recommended by ISO 8529-1[45]. For the ith sphere exposed in the qth reference field, the ratio $r_{i,q}$ between the delivered and the measured fluence is an indication of the accuracy of the response of that sphere in the energy range covered by that field. Considering a series of reference fields covering the interval from thermal to 20 MeV neutrons and the associated values of $r_{i,q}$, their average is expected to be around 1.00 and their standard deviation in the order of few per cent (3 % is a typical value for well-established BSS)[46, 47]. The accuracy of extended range spheres[44] may be evaluated using high-energy fields as those available at the CERF facility or the quasi-monoenergetic high-energy fields produced at TSL (Uppsala, Sweden) or at iThemba Labs (South Africa).

ACTIVE DETECTORS

Ref. (37) constitutes an excellent review of the general use of active counters. Popular active counters for BSSs are the 4 mm×4 mm cylindrical ^{6}LiI(Eu) scintillator and different types of ^{3}He-filled proportional counters. The ^{6}LiI(Eu) is very small, allowing one to use small spheres as the 2 in. and 2.5 in. but it is sensitive to photons, due to the high density and high atomic number of iodine. This can be corrected if the signal is acquired on a spectrometric chain, since the neutron peak has a nearly Gaussian shape and the photon background is an exponentially decreasing continuous function. ^{3}He-filled proportional counters have significantly lower

photon sensitivity and higher neutron efficiency. The cylindrical (10 mm×9 mm) ^{3}He-filled (8 kPa) proportional counter, type 05NH1, has twice the efficiency of ^{6}LiI(Eu). It is currently in use at UAB (Spain) and IRSN (France). The spherical (diameter 3.2 cm) ^{3}He-filled (200 kPa) proportional counter, type SP9 by Centronic Ltd. (UK), is a factor 10 more sensitive than ^{6}LiI(Eu). It is used at PTB, NPL, Helmholtz Zentrum München among other laboratories. For high-energy neutron fields, Vylet[48] used a 12.7×12.7 cm^2 organic scintillator, which is very convenient in the energy region >20 MeV due to the ^{12}C(n,2n)^{11}C activation of carbon (threshold 18 MeV).

An aspect that can be of interest for measurements around particle accelerators is the performance of these counters in pulsed fields. Often the primary beam is delivered in macro-pulses with a repetition rate in the order of 100 Hz and duration of microseconds to milliseconds. Each macro-pulse may comprise a micro-structure formed by pulses with a duration of approximate nanoseconds. Since the intrinsic dead-time of active counters (few μs) may be comparable with the duration of the macro-pulses, one could expect that a counter be unable to detect more than one neutron per macro-pulse. This is true if the counter is exposed without a surrounding moderator ('bare' configuration). Actually the counter performance improves if a sphere is used, because the arrival of thermalised neutrons at the central detector is spread over a time interval in the order of tens to hundreds of microseconds according to an exponential function (die-away effect). This is mainly due to the diffusion time of thermal neutrons in polyethylene, since the slowing down time from the initial energy to the thermal domain is relatively negligible. Consequently the die-away time constant T_d is only a function of the sphere diameter and its value ranges from about 30–140 μs when the sphere diameter increases from 2' to 12' and for a polyethylene density of 0.95 g cm^{-3}[49].

If a 7' sphere (T_d∼50 μs) is exposed in a neutron beam with a macro-pulse duration of 100 μs and repetition rate of 100 Hz, the 'arrival' rate at the central detector can be calculated and compared with the 'delivery' rate (i.e. the rate that a detector with zero dead-time and zero die-away time would indicate during the time interval where the beam is 'on'). This is done in Figure 4.

If the delivery rate is 5×10^4 s^{-1} and the detector dead-time is 5 μs, only 80 % of the events would be counted if T_d=0. In a more realistic case, with T_d∼50 μs, 88 % of the events is counted. It should be underlined that the simplified example presented above does not take into account that neutrons are also moderated in the materials surrounding the measurement system and adopts a pure non-paralysable model for the response of the counter.

Figure 4. Comparison between the 'delivery' rate and the 'arrival' for a 7' sphere (T_d∼50 μs) exposed in a pulsed neutron beam with pulse duration of 100 μs. The repetition rate is lower than <2 kHz in order to neglect the interference between pulses. The units in the Y axis are arbitrary.

However, it suggests that the knowledge of the beam time structure and of the die-away constant of the spheres can help in estimating the count loss in a given irradiation condition.

PASSIVE DETECTORS

BSSs equipped with passive detectors such as TLD pairs, nuclear track detectors or activation foils are used in accelerator workplaces, presenting some of the following characteristics: high intensity, pulsed time structure, intense photon component and large electromagnetic noise.

TLD pairs (^{6}LiF/^{7}LiF) are available in different formats with different thermal neutron sensitivity[50]. Since the neutron signal is obtained by difference, their use is not recommended in fields with a large photon component. Here the photon signal may account for a large fraction of the thermoluminescent signal, and small uncertainties in the TL readings could lead to a large uncertainty in the determination of the neutron signal. TLD pairs have been used in medical electron LINACs in off-axis areas[30, 51] and around high-energy particle accelerators, where their results were comparable with those obtained with a ^{6}Li(Eu) scintillator[31].

Photon-insensitive nuclear track detectors with adequate converters can be highly sensitive to thermal neutrons[39]. However, the etching and analysis procedure is time consuming and can be affected by saturation effects.

The passive detectors most suited for high-intensity fields are certainly the activation foils, due to

their insensitivity to photons, to the good knowledge of the cross sections and to the possibility to perform very precise measurements even with portable counters. Gold, indium and dysprosium foils have been used in BSS, but gold foils are probably the most popular. The Au-BSS exploits the reaction ^{197}Au(n,γ)^{198}Au and the beta and gamma emission from ^{198}Au ($T_{1/2}$=2.7 d; $E_{\beta max}$=0.96 MeV, E_{γ}=0.41 MeV). BSSs equipped with gold foils have been used at NPL[52], UAB[53], IRSN[54], INFN[32] and in the USA[55], mainly to determine neutron spectra in medical LINACs. Esposito *et al*. used gold foils and TLD pairs in the same set of spheres in a medical LINAC, with fully comparable results[30]. The response function for activation foil-based BSS is extended to the saturation specific activity per unit fluence rate as a function of neutron energy, and the typical value for gold is 0.4 cm^2 g^{-1} for the 8 in. sphere at 1 MeV. For a passive BSS using gold foils with diameter of 1.5 cm and thickness of 0.1 mm, the minimum detectable fluence rate was found to be in the order of 10^3–10^4 cm^{-2} s^{-1}[56], depending on the neutron spectrum, exposure time, exposure to counting delay and counting time. Increasing the foil thickness and diameter can lower this figure, but this would also increase self-absorption and anisotropy effects. The anisotropy of the activation foils, evidenced for the small spheres, is a potential source of uncertainty. The degree of anisotropy may be investigated by simulations or, experimentally, using a directional thermal beam[52]: at NPL a 9 % difference was found, for the 2.5 in. sphere, from the response with the foil parallel to the beam and the response with the foil normal to the beam. The foils were discs with a 2.3 cm diameter and 0.05 mm thickness. Differences <3 % were found by MCNP calculation for foils with a 1.5 cm diameter and 0.1 mm thickness[53]. Gold foils are practically insensitive to photons, provided that corrections are made for the following effects:

- the photons of the ^{196}Au (356 keV at 88 %, 333 keV at 23 % and 426 keV at 6.7 %) generated by the ^{197}Au(γ,n)^{196}Au reactions (threshold photon energy of 8.07 MeV);
- the photon-induced neutrons in polyethylene (threshold photon energy 18 MeV);
- the photon-induced neutrons in the metal of extended range spheres (threshold ∼8–10 MeV).

The calibration of the Au-BSS is usually done with a bare ^{252}Cf source in a low-scatter room.

Due to the usually simple geometry, the response matrix of a Au-BSS can be accurately simulated with Monte Carlo codes. Its overall uncertainty, estimable on the basis of irradiations in quasi-monoenergetic neutron fields, can be as low as 3 %[56].

Indium foils are also used[57], exploiting the reaction ^{115}In(n,γ)^{116m}In and the beta and gamma emission from ^{116m}In ($T_{1/2}$=54 m; $E_{\beta max}$=0.6 MeV–1.0 MeV; E_{γ}=0.4–1.3 MeV). The counting rate is much higher than for gold foils, but the very short half-life may constitute a serious limitation for operational measurements.

Dysprosium foils probably provide the optimal compromise for operational measurements. The exploited isotope is ^{164}Dy (28.2 % abundance in natural dysprosium). ^{165}Dy is a beta and gamma emitter with $E_{\beta max}$=1.3 MeV and $T_{1/2}$=2.334 h. The cross section is significantly higher than for gold (∼2700 barn at thermal energy, to be compared with the 98.8 barn of ^{197}Au). The Dy-BSS in use at INFN[33] is based on foils with a 1.2 cm diameter and 0.1 mm thickness that are analysed with a portable beta counter. The impact of parasitic (n,γ) and (γ,n) reactions on the beta counting has been investigated in different neutron fields, including high-energy fields, and no significant perturbations have been found in practice.

This system has been used to measure the neutron spectra from a spallation source[34] and a fusion based generator (R. Bedogni et al., submitted for publication). In the latter experiment, the Dy-BSS has been compared with the active ^{6}LiI(Eu)-based BSS, with fully consistent results.

Since activation foils are sensitive to the fluence rate and its time variations, the impact of pulsed beam time structures on their response should be evaluated. Ideally, the half-life of the activation product should be large enough to 'ignore' the time structure of the pulsed beams. In this case, the saturation activity may be calculated under the hypothesis that the total neutron fluence is delivered at a constant rate; see the following equation:

$$A_n = A_{sat}\frac{T_{on}}{T_{on}+T_{off}}\left[1-2^{-n(T_{on}+T_{off})/T_{1/2}}\right] \qquad (2)$$

A_n is the foil activity after the nth pulse; A_{sat} the saturation activity corresponding to the fluence rate in the 'on' period; T_{on} the pulse duration; T_{off} the time interval between two pulses; $T_{1/2}$ the half-life.

In reality, the activation is discrete and the activity increases as in the following equation:

$$A_n = A_{n-1} + (A_{sat} - A_{n-1})\cdot(1-2^{-T_{on}/T_{1/2}})\cdot 2^{-T_{off}/T_{1/2}} \qquad (3)$$

The continuous irradiation approximation tends to under-estimate the exact calculation.

CHOOSING THE SPHERES

The unfolding problem in Bonner sphere spectrometry is under-determined, because the number of mathematical functions that could reproduce a given set of measured sphere counts is theoretically infinite. In principle, the spectrometric information increases as the number of spheres increases, but the amount of added information decreases for each added sphere, because the response functions are not completely independent. Indeed, they present overlapping and similarities.

The information contained in a set of BSS measurements can be condensed in a curve representing the sphere reading as a function of the sphere diameter. For workplace spectra with a maximum energy of 20 MeV and for polyethylene spheres, this curve can be fitted with a smooth, non-oscillating, cubic spline interpolation[37]. The fact that a few well-chosen spheres (five to six) are enough to fully describe the curve means that the totality of the spectrometric information obtainable with this technique is provided by this minimum set of spheres. Clearly, since the measurements are affected by uncertainties, more spheres are recommended to produce more stable results. This also explains why the importance of the pre-information, in the form of a detailed *a priori* spectrum or a predefined parameterisation of the spectral components, is always very high and has very little dependence on the number of spheres (provided the minimum set is achieved).

The situation is even worse in the high-energy domain (>20 MeV), because the responses of all known designs of extended-range spheres have the same shape, as shown in Figure 5. Thus, the spectral information obtainable in the high-energy domain is quite uncertain[58]. It is therefore advisable, more than increasing the number of spheres, to investigate new detectors characterised by different shapes in the high-energy response.

Fission detectors or fission radiators, some of them being characterised by a threshold in the fission cross section, may help solve this problem. This can be evidenced with the following theoretical exercise. The high-energy spectrum shown in Figure 5 was folded with two response matrices:

(1) Eight polyethylene spheres+three extended range spheres (the set which response matrix is reported in Figure 5);
(2) Seven polyethylene spheres+four idealised detectors with step-wise response at 30, 45, 60 and 70 MeV.

The corresponding sets of sphere readings were unfolded using the FRUIT parametric unfolding code[59]. This code includes a statistics tool that derives, for each of the parameters describing the final spectrum, a probability distribution from which

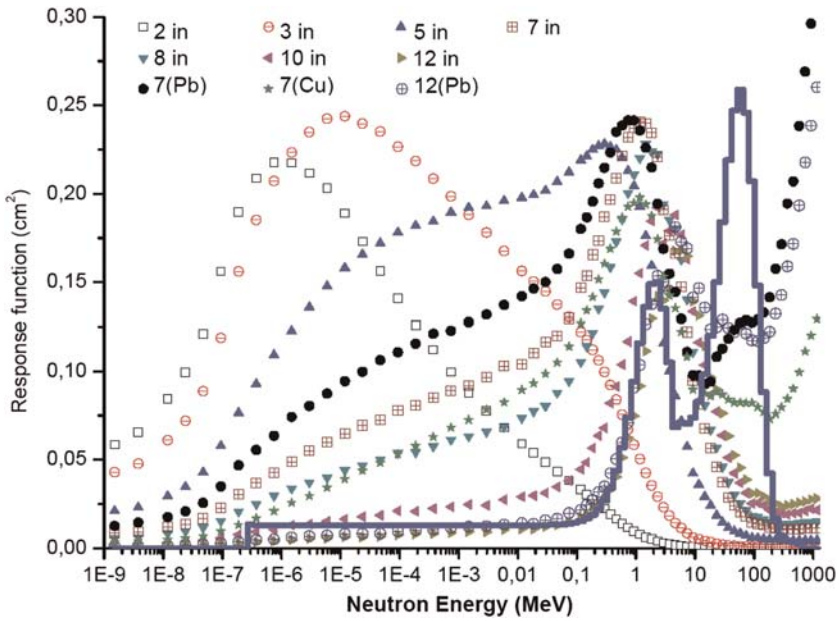

Figure 5. Typical response matrix of a BSS with extended range spheres superposed to a typical neutron spectrum of a high-energy field (in equi-lethargy representation). The response matrix refers to the INFN-LNF ERBSS.

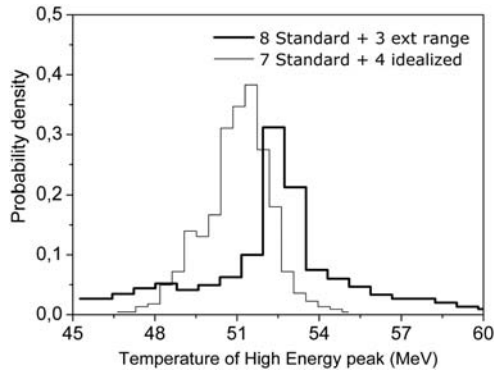

Figure 6. Probability distribution for the high-energy temperature (assuming an evaporation-like model for the high-energy peak).

the uncertainty on that parameter can be estimated. The distribution is calculated by automatically unfolding a large number of sphere reading sets, obtained by applying a Gaussian perturbation to the original set of sphere readings. The amplitude of this perturbation is a quadratic combination of the counting uncertainties, the response matrix overall uncertainty and any other source of uncertainty that may randomly affect the sphere readings. After the unfolding, the value of each parameter (among other spectrum-integrated quantities) is collected in a distribution.

In the 'high-energy hadron' model, FRUIT describes the high-energy peak with an evaporation-like curve, fully described by only two parameters: the fraction of fluence and the peak temperature. This model was found to be accurate enough to fit the high-energy spectra encountered behind thick shielding in high-energy particle accelerators. The peak temperature multiplied by 2 gives the peak position. Figure 6 shows the distributions for the peak temperature obtained in cases (1) and (2).

As expected, the presence of step-wise response functions implies a better determination of the peak temperature. This was estimated to be 52 MeV with a standard deviation of 6 % for the standard ERBSS and 51 MeV (s.d. 2 %) for the idealised response matrix.

UNFOLDING

A very important aspect of operational measurements with the BSS is a consistent estimation of the uncertainties affecting the BSS counts and the use of an unfolding algorithm that allows taking uncertainties into account. The propagation of uncertainties in the unfolding process is not direct and is performed by very few of the available codes, as those based on the Bayesian approach[60], MAXED[61] and FRUIT[59].

In the unfolding process, very small variations in the input data may produce large changes in the resulting spectrum, requiring the adoption of specific experimental procedures to reduce uncertainties to the maximum extent. As an example, if measurements with an activation foil-based BSS are done in an accelerator, the estimation of the saturation factor on the basis of the instantaneous beam intensity, rather than considering an average intensity, will improve the accuracy of the BSS data. The neutron field should be monitored in terms of time variability but also in terms of direction and energy variability. The uncertainty due to small instabilities in the energy distribution of the field may be evaluated by exposing at least two monitor instruments having very different energy dependence of the response, such as an extended-range and a 3' sphere. Monitor instruments placed at different angles with respect to the reference line-of-flight may be useful to estimate the uncertainty due to small instabilities in the direction distribution of the field[28]. An important source of uncertainty is the response matrix, the overall uncertainty of which should be estimated in well-known neutron fields (see the section The response of the BSS). Besides the uncertainties due to the simulation model (dimensions, densities, compositions, cross sections), there are other factors that may affect the response of a BSS. As an example, if measurements in collimated beams are performed, the response matrix should be corrected to consider the beam dimension. An example of such a correction is shown in ref. (34).

The anisotropy of the central detector, especially in an activation foil-based BSS, may constitute a source of uncertainty. If the direction distribution of the field is known, appropriate corrections can be applied to the response matrix. Otherwise, an additional uncertainty should be associated with the reading of the small spheres.

A potential source of systematic errors is the decrease with time of the efficiency of the central detector. ^{3}He or ^{6}LiI(Eu) detectors are stable, but small variation in the order of a fraction of % per year can be expected. Very simple devices can be used to check this parameter, such as a polyethylene moderator where the detector and a small neutron source are allocated in fixed geometry. The dead-time and the photon sensitivity of the counter should also be known.

Provided that the response matrix is well known and all major sources of uncertainty are controlled, the unfolding is the most complex step of the spectrometry task.

The topic of unfolding is treated in detail elsewhere[59–63]. A number of unfolding codes have characteristics that make them hard to use in

operational radiation protection monitoring. These are the complexity of the codes, the need for a very expert user and the need for realistic *a priori* information, such as a 'default spectrum' as close as possible to the expected spectrum.

A way to eliminate the need for a detailed *a priori* spectrum is the parametric approach, used in FRUIT and in the Bayesian methods. The parametric approach eliminates the non-physical solutions by modelling the neutron spectrum as a superposition of elementary spectra parameterised in terms of a small number (about 10) of physically meaningful parameters.

As an example (referred to FRUIT), besides the sphere response functions, the counts and related uncertainties, the user is only asked to introduce qualitative information on the type of 'radiation environment', on the basis of a check-box input section. The available models are fission, evaporation, narrow-spectrum (suited for mono-chromatic fields) and, for high-energy particle accelerators, 'high-energy hadron' and 'high-energy electron' accelerators. While the 'hadron' model is mostly suited for shielded areas, being the high-energy peak fitted with an evaporation-like curve, the 'electron' model implements specific functions to reproduce the mid-energy neutrons from quasi-deuteron effect and high-energy neutrons from photo-pion production[64].

No 'default spectrum' is asked of the user. The code randomly generates a default spectrum, needed to start the iterative procedure, on the basis of the radiation environment selected by the user. Taking advantage of a 'flexible tolerance' convergence mechanism, results do not depend on the numerical values of this spectrum. Other aspects are as follows:

- The user intervenes to control the convergence procedure. The code is not intended as a 'black box'.
- User friendliness and visual operation. The quantities involved in the unfolding process and their variation are continuously displayed: the plot of the spectrum, the measured and unfolded Bonner sphere counts, the parameters, the tolerances and the dosimetric quantities.
- The code includes a statistics tool that derives, for each of the parameters describing the final spectrum, a probability distribution from which the uncertainty on that parameter can be estimated. This analysis is done for the parameters, the fluence (and fractions of fluence in given energy intervals) and the ambient dose equivalent. Uncertainties are also derived for the numerical values of the spectrum. Uncertainties of input quantities (sphere counts, response matrix and other sources that may randomly affect the sphere counts) are used to perform these analyses.

The mentioned CONRAD inter-comparison[35] allowed comparing different BSSs (all using extended-range spheres) and different unfolding codes in a high-energy problem. The codes were FRUIT, the Bayesian method used to produce a guess spectrum for MAXED, MAXED and a variation of SAND called MSANDB [65].

The systems provided integral results with a very low dispersion (<6 % for $H^*(10)$ and <3 % for Φ), while the uncertainties provided by each group were <5 % for Φ and <10 % for $H^*(10)$. Good agreement was found in the overall shape of the spectra, with the largest differences observed in the high-energy peak. This was expected due to the low resolution of the ERBSS in this region. However, some difference could be attributed to the different unfolding codes (with different ways to introduce pre-information) and to different validation of the BSS.

CONCLUSIONS

The use of neutron spectrometry techniques is increasing, not only in research applications, but also in routine radiation protection of neutron-producing facilities.

Workplace neutron fields are very different in terms of energy range (from thermal up to hundreds of MeV), intensity, time structure, presence of photon radiation and electromagnetic noise. To date, Bonner Sphere Spectrometry is the technique that best covers such a variety of workplaces. Features such as the response over a broad energy interval (up to hundreds MeV when metal-loaded spheres are used) and the availability of active and passive detectors, with different neutron response and gamma discrimination characteristics, make this spectrometer still irreplaceable.

The use of the BSS (ERBSS for high-energy facilities) is rather well harmonised and different BSSs with different unfolding codes and pre-information are able to give the same integral values (within limited spread) and comparable spectra in a workplace field. However, there are aspects requiring further analysis, such as the use of unfolding codes (and the influence of the pre-information) and how different can be the results of BSSs having different experimental validation. Open problems of the high-energy region are the following:

(1) The simulation codes rely on models to describe the high-energy region, and these models have been partially verified with experiments. On the other hand, the response matrices of the ERBSS are calculated using the same codes, thus

producing a correlation between the BSS results and the simulated spectra.

(2) The limited availability of high-energy reference fields[66] and the difficulty in obtaining accurate spectrometric measurements over the whole energy range.

(3) With the current design of extended range spheres, only limited information may be obtained on the high-energy component of the field. New designs with different shape of the high-energy response would be highly valuable.

Passive BSSs or ERBSSs play an important role in the characterisation of fields with high-intensity, pulsed-time structure or large photon background. This is the case of radiotherapy facilities based on electrons or hadrons, nuclear reactors, research or industrial particle accelerators (with special attention to the increasing number of beams devoted to chip irradiation and material studies), and new laser-based acceleration techniques.

Activation-foil based systems have been well characterised by different groups and constitute a mature technique. A problem is their experimental validation, due to the limited availability of reference fields with adequate intensity. As done in the past for active BSSs, an inter-comparison campaign for passive systems using different configurations or activation foils would be very important to harmonise their use and evaluate the response matrices calculated in each group.

REFERENCES

1. Swanson, W. P. and Thomas, R. H. *Dosimetry for radiological protection at high-energy particle accelerators*. In: The Dosimetry of Ionizing Radiation, Vol. III. Kase, K. R., Bjarngard, B. and Attix, F. H., Eds. Academic Press (1990).
2. McDonald, J. C. *Determination of personal dose equivalents in accelerator radiation fields*. Radiat. Prot. Dosim. **96**(4), 423–427 (2001).
3. ICRP. *Recommendations of the International Commission on Radiological Protection*. ICRP Publication 60. Pergamon Press (1991).
4. NCRP. *Radiation protection for particle accelerator facilities*. NCRP Report 144. National Council on Radiation Protection and Measurements (2004).
5. Silari, M. *Workplace characterization in mixed neutron-gamma fields, specific requirements and available methods at high-energy accelerators*. Radiat. Prot. Dosim. **124**(3), 230–244 (2007).
6. Mitaroff, A. and Silari, M. *The CERN-EU high-energy reference field (CERF) facility for dosimetry at commercial flight altitudes and in space*. Radiat. Prot. Dosim. **102**(3), 7–22 (2002).
7. ICRP. *Conversion coefficients for use in radiological protection against external radiation*. ICRP Publication 74. Pergamon Press (1996).
8. ICRU. *Conversion coefficients for use in radiological protection against external radiation*. ICRU Report 57. International Commission on Radiation Units and Measurements (1998).
9. Burgkhardt, B., Fieg, G., Klett, A., Plewnia, A. and Siebert, B. R. L. *The neutron fluence and H*(10) response of the new LB 6411 Rem counter*. Radiat. Prot. Dosim. **70**(1–4), 361–364 (1997).
10. Birattari, C., Ferrari, A., Nuccetelli, C., Pelliccioni, M. and Silari, M. *An extended range neutron rem counter*. Nucl. Instrum. Methods **A297**, 250–257 (1990).
11. Olsher, R. H., Hsu, H. H., Beverding, A., Kleck, J. H., Casson, W. H., Vasilik, D. G. and Devine, R. T. *WENDI: an improved neutron rem meter*. Health Phys. **79**, 170–181 (2000).
12. Klett, A., Mayer, S., Theis, C. and Vincke, H. *A neutron dose rate monitor for high energies*. Radiat. Meas. **41**, S279–S282 (2007).
13. Mayer, S., Forkel-Wirth, D., Fuerstner, M., Menzel, H. G., Mueller, M. J., Perrin, D., Theis, C. and Vincke, H. *Response of neutron detectors to high-energy mixed radiation fields*. Radiat. Prot. Dosim. **125**(1–4), 289–292 (2007).
14. Silari, M. *et al*. *Intercomparison of radiation protection devices in a high-energy stray neutron field. Part III: Instrument response*. Radiat. Meas. **44**, 660–672 (2009).
15. d'Errico, F. and Bos, A. J. *Passive detectors for neutron personal dosimetry: state of the art*. Radiat. Prot. Dosim. **110**(1–4), 195–200 (2004).
16. ICRU. *Determination of operational dose equivalent quantities for neutrons*. ICRU Report 66. International Commission on Radiation Units and Measurements (2001).
17. Gomez-Ros, J. M., Bedogni, R., Moraleda, M., Delgado, A., Romero, A. and Esposito, A. *A multi-detector neutron spectrometer with nearly isotropic response for environmental and workplace monitoring*. Nucl. Instrum. Methods Phys. Res. A **613**, 127–133 (2010).
18. Gomez-Ros, J. M., Bedogni, R., Moraleda, M., Romero, A., Delgado, A. and Esposito, A. *Design and validation of a single sphere multidetector neutron spectrometer based on LiF:Mg,Cu,P thermoluminescence dosimeters*. Radiat. Meas. **45**(10), 1220–1223 (2010).
19. Thomas, D. J. and Klein, H., Eds. *Neutron and photon spectrometry techniques for radiation protection*. Radiat. Prot. Dosim. **107**(1–3), 155–174 (2003).
20. Lindborg, L. *et al*. *Application of workplace correction factors to dosemeter results for the assessment of personal doses at nuclear facilities*. Radiat. Prot. Dosim. **124**(3), 213–218 (2007).
21. ISO. *Reference radiation fields—simulated workplace neutron fields—Part 1: characteristics and methods of production*. ISO 12789–1. International Organization for Standardization (2008).
22. ISO. *Reference radiation fields—simulated workplace neutron fields—Part 2: calibration fundamentals related to the basic quantities*. ISO 12789–2. International Organization for Standardization (2008).
23. Bartlett, D. T., Chartier, J. L., Matzke, M., Rimpler, A. and Thomas, D. J. *Concepts and quantities in spectrometry and radiation protection*. Radiat. Prot. Dosim. **107**(1–3), 23–35 (2003).

24. Thomas, D.J. *Neutron spectrometry for radiation protection*. Radiat. Prot. Dosim. **110**(1–4), 141–149 (2004).
25. Thomas, D. J. and Alevra, A. V. *Bonner sphere spectrometers—a critical review*. Nucl. Instrum. Methods Phys. Res. A **476**, 12–20 (2002).
26. Vylet, V., Liu, J. C., Rokni, S. H. and Thai, L.-X. *Measurements of neutron spectra at the Stanford linear accelerator center*. Radiat. Prot. Dosim. **70**(1–4), 425–428 (1997).
27. Wiegel, B. and Alevra, A. V. *NEMUS—the PTB neutron multisphere spectrometer: Bonner spheres and more*. Nucl. Instrum. Methods A **476**, 36–41 (2002).
28. Esposito, A., Bedogni, R., Domingo, C., García, M. J. and Amgarou, K. *Measurements of leakage neutron spectra from a high-energy positron accumulation ring using extended-range Bonner Sphere Spectrometers*. Radiat. Meas. **45**(10), 1522–1525 (2010).
29. Bedogni, R. *Neutron spectrometry and dosimetry for radiation protection around a high energy electron/positron collider*. Ph.D. thesis, Universidad Autonoma de Barcelona, Barcelona, Spain (2006).
30. Esposito, A., Bedogni, R., Lembo, L. and Morelli, M. *Determination of the neutron spectra around a 18 MV medical LINAC with a passive Bonner sphere spectrometer based on gold foils and TLD pairs*. Radiat. Meas. **43**, 1038–1043 (2008).
31. Bedogni, R., Esposito, A. and Chiti, M. *Determination of workplace neutron spectra at a high energy hadron accelerator using active and passive Bonner sphere spectrometers*. Radiat. Meas. **43**, 1113–1117 (2008).
32. Bedogni, R., Esposito, A., Gentile, A., Angelone, M. and Gualdrini, G. *Determination of the response matrix for a passive Bonner spere spectrometer based on gold foils*. Radiat. Meas. **43**, 1104–1107 (2008).
33. Bedogni, R., Ferrari, P., Gualdrini, G. and Esposito, A. *Design and experimental validation of a Bonner Sphere Spectrometer based on Dysprosium activation foils*. Radiat. Meas. **45**(10), 1021–1204 (2010).
34. Bedogni, R., Esposito, A. and Gomez-Ros, J. M. *Response matrix of an Extended Range Bonner Sphere Spectrometer for the characterization of collimated neutron beams*. Radiat. Meas. **45**(10), 1005–1212 (2010).
35. Wiegel, B. *et al*. *Intercomparison of radiation protection devices in a high-energy stray neutron field. Part II: Bonner sphere spectrometry*. Radiat. Meas. **44**, 673–691 (2009).
36. Reginatto, M. *Resolving power of a multisphere neutron spectrometer*. Nucl. Instrum. Methods Phys. Res. A **480**, 690–695 (2002).
37. Alevra, A. V. and Thomas, D. J. *Neutron spectrometry in mixed fields: multisphere spectrometers*. Radiat. Prot. Dosim. **107**(1–3), 37–72 (2003).
38. Gualdrini, G. *et al*. *Analysis of the CONRAD computational problems expressing only stochastic uncertainties: neutrons and protons*. Radiat. Prot. Dosim. **131**(1), 7–14 (2008).
39. Fassò, A., Ferrari, A., Ranft, J. and Sala, P. R. FLUKA: A Multi-Particle Transport Code. CERN-2005-10,INFN/TC_05/11,SLAC-R-773 (2005).
40. Battistoni, G., Muraro, S., Sala, P. R., Cerutti, F., Ferrari, A., Roesler, S., Fassò, A. and Ranft, J. In: Proceedings of the Hadronic Shower Simulation Workshop 2006. Albrow, M. and Raja, R. Eds, Fermilab, 6–8 September 2006, AIP Conference Proceeding 896, pp. 31 (2007).
41. Garny, S., Mares, V. and Rühm, W. *Response functions of a Bonner sphere spectrometer calculated with GEANT.4*. Nucl. Instrum. Methods Phys. Res. A **604**, 612–617 (2009).
42. Van der Meer, K., Goldberg, M.-B., Lehmann, E. H. *et al*. *Spallation yields of neutrons produced in thick lead/bismuth targets by protons at incident energies of 420 and 590 MeV*. Nucl. Instrum. Methods B **217**, 202–220 (2004).
43. Rollet, S., Agosteo, S., Fehrenbacher, G., Hranitzky, C., Radon, T. and Wind, M. *Intercomparison of radiation protection devices in a high-energy stray neutron field, Part I: Monte Carlo simulations*. Radiat. Meas. **44**, 649–659 (2009).
44. Birattari, C., Dimovasili, E., Mitaroff, A. and Silari, M. *A Bonner Sphere Spectrometer with extended response matrix*. Nucl. Instrum. Methods Phys. Res. A **620**(2–3), 260–269 (2010).
45. ISO. *Reference neutron radiations—Part 1: Characteristics and methods of production*. ISO 8529–1. International Organization for Standardization (2001).
46. Lacoste, V., Gressier, V., Pochat, J.-L., Fernández, F., Bakali, M. and Bouassoule, T. *Characterization of Bonner Sphere systems at monoenergetic and thermal neutron fields*. Radiat. Prot. Dosim. **110**(1–4), 529–532 (2004).
47. Bedogni, R., Domingo, C., Esposito, A., Chiti, M., Garcia Fusté, M. J. and Lovestam, G. *Testing Bonner Sphere Spectrometers in the JRC-IRMM mono-energetic neutron beams*. Nucl. Instrum. Methods Phys. Res. A **620**, 391–396 (2010).
48. Vylet, V. *Response matrix of an extended Bonner sphere system*. Nucl. Instrum. Methods A **476**, 26–30 (2002).
49. Woznicka, U., Drozdowicz, K. and and Dabrowska, J. *A generalized interpretation of buckling experiments for thermal neutrons*. Nucl. Instrum. Methods Phys. Res. A **455**, 660–669 (2000).
50. Bedogni, R., Esposito, A., Angelone, M. and Chiti, M. *Determination of the response to photons and thermal neutrons of new LiF based TL materials for radiation protection purposes*. IEEE Trans. Nucl. Sci. **53**(3), 1367–1370 (2006).
51. Barquero, R., Mendez, R., Vega-Carrillo, H. R., Iñiguez, M. P. and Edwards, T. M. *Neutron spectra and dosimetric features around an 18 MV LINAC accelerator*. Health Phys. **88**(1), 48–58 (2005).
52. Thomas, D. J., Hawkes, N. P., Jones, L. N., Kolkowski, P. and Roberts, N. J. *Characterization and utilizatin of a Bonner sphere set based on gold activation foils*. Radiat. Prot. Dosim. **126**(1–4), 229–233 (2007).
53. Fernandez, F., Bouassoule, T., Amgarou, K., Domingo, C., Garcia, M. J., Lacoste, V., Gressier, V. and Muller, H. *Monte Carlo calculation and validation of a gold foil-based Bonner sphere system*. Radiat. Prot. Dosim. **126**(1–4), 366–370 (2007).
54. Amgarou, K., Lacoste, V., Muller, H. and Fernandez, F. *Set-up of a passive Bonner sphere system for neutron spectrometry at mixed fields with predominant photon component based on activation detector*. Radiat. Prot. Dosim. **126**(1–4), 337–341 (2007).

55. Wang, Z., Hutchinson, J. D., Hertel, N. E., Burgett, E. and Howell, R. M. *Study of a gold-foil-based multisphere neutron spectrometer*. Radiat. Prot. Dosim. **128**(3), 289–293 (2008).
56. Garcia Fusté, M. J. *Neutron spectrometry in complex n-γ fields—Application to LINAC and PET facilities*. PhD thesis, Universitat Autonoma de Barcelona, Bellaterra, Spain (2010).
57. Wang, Z., Howell, R. M., Burgett, E. A., Kry, S. F., Hertel, N. E. and Salehpour, M. *Calibration of indium response functions in an Au-In-BSE system up to 800 MeV*. Radiat. Prot. Dosim. **139**(4), 565–573 (2010).
58. Reginatto, M. *What can we learn about the spectrum of high-energy stray neutron fields from Bonner sphere measurements?*. Radiat. Meas. **44**, 692–699 (2009).
59. Bedogni, R., Domingo, C., Esposito, A. and Fernández, F. *FRUIT: an operational tool for multisphere neutron spectrometry in workplaces*. Nucl. Instrum. Methods A **580**, 1301–1309 (2007).
60. Reginatto, M. *Bayeasian approach for quantifying the uncertainty of neutron doses derived from spectrometric measurements*. Radiat. Prot. Dosim. **121**(1), 64–69 (2006).
61. Reginatto, M. and Goldhagen, P. *A computer code for the deconvolution of multisphere neutron spectrometer data using the maximum entropy method*. Report EML-595. Environmental Measurement Laboratory (1998).
62. Matzke, M. *Unfolding procedures*. Radiat. Prot. Dosim. **107**(1–3), 155–174 (2003).
63. Reginatto, M. *Overview of spectral unfolding techniques and uncertainty estimation*. Radiat. Meas. **45**(10), 1323–1329 (2010).
64. Bedogni, R., Pelliccioni, M. and Esposito, A. *A parametric model to describe neutron spectra around high-energy electron accelerators and its application in neutron spectrometry with Bonner Spheres*. Nucl. Instrum. Methods A **615**, 78–82 (2010).
65. Simmer, G., Mares, V., Weitzenegger, E. and Rühm, W. *Iterative unfolding for Bonner sphere spectrometers using the MSANDB code—Sensitivity analysis and dose calculation*. Radiat. Meas. **45**(1), 1–9 (2010).
66. Lacoste, V. *Review of radiation sources, calibration facilities and simulated workplace fields*. Radiat. Meas. **45**(10), 1083–1089 (2010).